analytical chemistry

Article

pubs.acs.org/ac

Chemical Functionalization of Germanium with Dextran Brushes for Immobilization of Proteins Revealed by Attenuated Total Reflection Fourier Transform Infrared Difference Spectroscopy

Jonas Schartner, Nina Hoeck, Jörn Güldenhaupt, Laven Mavarani, Andreas Nabers, Klaus Gerwert, and Carsten Kötting*

Department of Biophysics, Faculty of Biology and Biotechnology, Ruhr-University, 44801 Bochum, Germany

Supporting Information

ABSTRACT: Protein immobilization studied by attenuated total reflection Fourier transform infrared (ATR-FT-IR) difference spectroscopy is an emerging field enabling the study of proteins at atomic detail. Gold or glass surfaces are frequently used for protein immobilization. Here, we present an alternative method for protein immobilization on germanium. Because of its high refractive index and broad spectral window germanium is the best material for ATR-FT-IR spectroscopy of thin layers. So far, this technique was mainly used for protein monolayers, which lead to a limited signal-to-noise ratio. Further, undesired protein−protein interactions can occur in a dense layer. Here, the germanium surface was functionalized with thiols and stepwise a dextran brush was generated. Each step was monitored by ATR-FT-IR spectroscopy. We compared a 70 kDa dextran with a 500 kDa dextran regarding the binding properties. All surfaces were characterized by atomic force microscopy, revealing thicknesses between 40 and 110 nm. To analyze the capability of our system we utilized N-Ras on mono-NTA (nitrilotriacetic acid) functionalized dextran, and the amount of immobilized Ras corresponded to several monolayers. The protein stability and loading capacity was further improved by means of tris-NTA for immobilization. Small-molecule-induced changes were revealed with an over 3 times higher signal-to-noise ratio compared to monolayers. This improvement may allow the observation of very small and so far hidden changes in proteins upon stimulus. Furthermore, we immobilized green fluorescent protein (GFP) and mCherry simultaneously enabling an analysis of the surface by fluorescence microscopy. The absence of a Förster resonance energy transfer (FRET) signal demonstrated a large protein−protein distance, indicating an even distribution of the protein within the dextran.

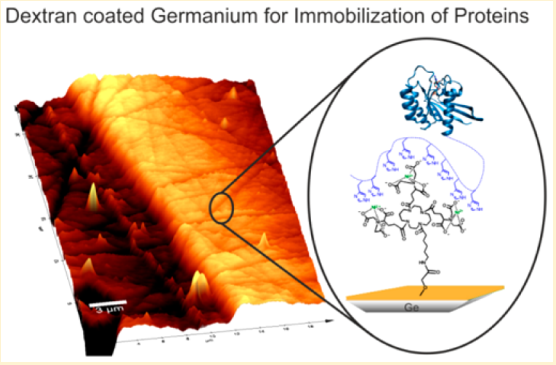

Fourier transform infrared (FT-IR) spectroscopy is an important tool to unravel the reaction mechanism of proteins with atomic detail. Conformational changes and the involvement of crucial residues (e.g., amino acids or phosphates) can be monitored in real time without any label.[1−7] The development of biosensors and new immobilization techniques is a growing and powerful field. Attenuated total reflection Fourier transform infrared (ATR-FT-IR) spectroscopy with germanium as internal reflection element provides an excellent signal-to-noise ratio. Immobilization of GTPases with lipid anchors on germanium with self-assembled lipid bilayers allowed measurements in their physiological environment.[8−10] Still the most popular method for studying interactions of immobilized proteins is surface plasmon resonance (SPR), and a complete setup with chemically functionalized gold surfaces is commercially available.[11−13] The use of dextran brushes for protein immobilization on gold surfaces was established by Löfas and Johnsson, and it is widely used for studying immobilized proteins.[14−19] In addition, gold nanoparticles have been dextran-coated for biomolecule immobilization.[20] Besides, gold borosilicate glass surfaces were used for protein immobilization via functionalized dextran molecules.[21−23] On germanium only the interaction of adsorbed proteins with dextran in solution has been investigated.[24] As a capturing group for the protein immobilization, histidine tags are reliable and efficient.[25−27] The common usage of histidine tags for purification of proteins makes almost every protein accessible without further treatment or chemical modification. Protein immobilization stability can be improved when tris-NTA (nitrilotriacetic acid) is employed for the attachment.[28−30] Nevertheless, SPR and related methods lack spectral resolution, which is crucial to reveal protein integrity and changes upon stimulus. We recently developed a universal immobilization technique on germanium by employing triethoxysilanes.[31] Furthermore, we established the use of thiols for protein immobilization on germanium.[32] Here, we developed a covalent and stable functionalization of

Received: May 15, 2015
Accepted: June 23, 2015
Published: June 23, 2015

DOI: 10.1021/acs.analchem.5b01823
Anal. Chem. 2015, 87, 7467−7475

germanium with dextran brushes. The high stability of the thiol-self-assembled monolayer (thiol-SAM) enabled the covalent attachment of dextran brushes even under harsh conditions, which would be almost impossible on silane-modified germanium surfaces.[32,33] Large amounts of N-Ras were attached on different dextran surfaces corresponding to several protein monolayers. Upon treatment with the small molecule beryllium fluoride, difference spectra with an outstanding signal-to-noise (S/N) ratio were obtained. By using tris-NTA-modified dextran brushes protein stability was further increased. The green fluorescent protein (GFP) was immobilized simultaneously with the red fluorescent protein mCherry, and we measured a homogeneous contribution of both dyes. In summary, we present a method to immobilize proteins on dextran-coated germanium crystals, which detects even small changes in proteins upon stimulus with atomic detail.

EXPERIMENTAL SECTION

All chemicals and organic solvents were purchased from Sigma-Aldrich (Taufkirchen, Germany). N-Ras1-180 with a deca-histidine tag was expressed as described previously.[31] mCherry was expressed and purified as described elsewhere.[32] The green fluorescent protein was expressed and purified as described previously.[34]

ATR-FT-IR. ATR-FT-IR spectroscopic measurements were performed as described previously.[9,31] If not stated otherwise, spectra were recorded with a spectral resolution of 2 cm^{-1} and a scanner velocity of 80 kHz. The spectra of the tris-ANTA (aminonitrilotriacetic acid) coupling were water vapor corrected, negative water bands were subtracted, and a moving average (10 cm^{-1}) to increase the S/N ratio was performed.

Germanium Pretreatment. Germanium pretreatment was performed as described previously.[31] The internal reflection elements (IREs) were 52 mm × 20 mm × 2 mm trapezoidal germanium ATR plates (Korth, Kiel, Germany) with an aperture angle of 45°. The germanium crystals were polished with 1.0 μm polishing solution for 30 min and with 0.1 μm polishing solution (Struers GmbH, Willich, Germany) at each side for 5 min. The thiolation procedure was published elsewhere.[32]

Dextran Coating. The protocol was modified based on Löfas and Johnsson.[14] A self-assembled 8-mercaptooctanol monolayer was washed with isopropyl alcohol (15 min), water (10 min), and finally immersed in 400 mM NaOH and 400 mM diethylene glycol dimethyl ether (5 min). Subsequently, 2 mL of epichlorohydrin (2.5 M) was added and allowed to react under circulation for 4 h. The resultant epoxylated surface was washed with water (8 min), ethanol (4 min), and water (8 min). The desired dextran was dissolved in 100 mM NaOH (70 kDa, 0.2 g/mL; 500 kDa, 0.1 g/mL) and flushed over the surface after recording a new reference spectrum. The dextran coating was done overnight before washed with water (20 min). For the carboxylation a solution of 1 M bromoacetic acid in 2 M NaOH was employed. After equilibration of the system with water a new reference was taken, and the reaction was performed for 4 or 16 h. The surface was washed with water (20 min), MES buffer (20 mM, 100 mM NaCl, pH 5.0, 10 min), and finally rinsed with a 250 mM *N*-(3-(dimethylamino)-propyl)-*N*′-ethylcarbodiimide (EDC)/100 mM *N*-hydroxysuccinimide (NHS) solution. A new reference was recorded, and after 1 h the surface was washed for 10 min with MES buffer. Subsequently, the system was equilibrated with a sodium phosphate buffer (50 mM NaP_i, pH 5.4) and a 50 mM aminonitrilotriactetic acid (mono-ANTA) solution (NaP_i, pH 5.4) was flushed over the germanium crystal. Again a new reference was taken, and the reaction was done for 2 or 16 h. Besides mono-NTA we employed tris-NTA for protein attachment and performed the reaction under the same buffer conditions with a 4 mM tris-ANTA solution for 16 h. Subsequently, the surface was washed with buffer (15 min) and blocked with 1 M ethanolamine (pH 8.5, 10 min). The NTA groups were loaded with 30 mM $NiCl_2$ (20 mM Hepes, 150 mM NaCl, pH 7.4) for 10 min. After washing with NaP_i buffer the surface was equilibrated with protein binding buffer.

Tris-ANTA Synthesis. Tris-ANTA was synthesis based on the protocol of Lata et al.[28] A brief synthesis scheme is presented in the Supporting Information (Scheme S1). The final product was characterized with electrospray ionization mass spectrometry (ESI-MS): $C_{43}H_{68}N_8O_{22}$, 1049 g/mol $[MH]^+$.

Tris-NTA Nickel Complexation. To analyze the coordination of the Ni^{2+} ion by the tris-NTA branches, the surface was washed 50 mM K_2SO_4 (pH 4.8) and a new reference spectrum was recorded. Subsequently, a 50 mM solution of $NiSO_4$ (pH 4.8) was employed and the changes were monitored after washing with K_2SO_4. After recording a new reference the surface was immersed with 50 mM ethylenediaminetetraacetic acid (EDTA) in K_2SO_4. The changes were observed after washing with K_2SO_4.

Atomic Force Microscopy. For the characterization of the dextran surface atomic force microscopy (AFM) with a WiTec Alpha300AR (WiTec Inc., Ulm, Germany) in contact mode was performed on different border regions of the surface. For the measurements, which were performed in buffer solution, contact mode probes (Al-coated, force constant 0.2 N/m) were used. A 20× water immersion objective was used. Areas presented are between 200 and 1100 μm^2. For the data analysis an N-order line subtraction was performed. Thereby, the line correction subtracts a polynom of a certain degree from each line of the scan. The polynom is adjusted by least-square method. Furthermore, the average height of the measured surface and the medium roughness of the layer are calculated. These values are visualized in the cross sections, which were displayed for each measurement. The cross sections are averaged over 3 μm. For the evaluation of the data WiTec Project software was used (version 2.08, WiTec Inc.).

Protein Immobilization. Protein-binding buffer 1 for the immobilization of N-Ras contained 20 mM Hepes (pH 7.4), 150 mM NaCl, 1 mM $NiCl_2$, 1 mM $MgCl_2$, and 0.1 mM GDP. For the immobilization of GFP and mCherry a 20 mM sodium phosphate buffer (pH 6.7, protein-binding buffer 2) was used.

Fluorescence Microscopy. For fluorescence measurements a BX41 microscope (Olympus, Hamburg, Germany) in combination with an X-cite 120Q UV lamp (Lumen Dynamics Group Inc., Canada) and an Olympus XC10 fluorescence camera was used. Fluorescence signals were measured through the quartz glass window (40 mm × 10 mm) of the ATR flow-through cell using a 100 times magnification and 25, 50, or 100 ms of exposure time. That is why the cuvette was removed from the sample compartment of the FT-IR spectrometer. GFP was excited through a band pass filter of 470−490 nm, and emission was detected through a 520 nm long pass filter. mCherry was excited through a band pass filter of 545−585 nm, and emission was observed through a 610 nm long pass filter. The fluorescence intensity was calculated by the integrated signal intensity (RGB value) over 10 random selected areas (each area

DOI: 10.1021/acs.analchem.5b01823
Anal. Chem. 2015, 87, 7467−7475

655 μm × 873 μm). These results were averaged. The quantum efficiency of the XC10 fluorescence camera (Olympus, Hamburg, Germany) was identical for both green and red pixels in the RGB mode. Thus, we could quantify the fluorescence intensities of both channels and determine the relative relation of both pixels to each other. Subsequently, the flow-cell was reinserted in the FT-IR spectrometer.

RESULTS AND DISCUSSION

Here, we report on the chemical functionalization of germanium with dextran brushes. The steps of this process are summarized in Scheme 1. At first a thiol monolayer of 8-mercaptooctanol was assembled according to the literature.[32,33] The hydroxyl-terminated surface was epoxylated, dextran-coated, carboxylated, and finally functionalized for specific immobilization of proteins. All steps were monitored label-free in real time with ATR-FT-IR spectroscopy, and the dextran-coated surfaces were further investigated by AFM. The use of dextran brushes overcomes the limitations of monolayers and enables an increased amount of immobilized protein in the detection volume which results in a significant increase in the signal-to-noise ratio. The three-dimensional (3D) structure of the generated dextran brush enables the accessibility of all immobilized protein for reaction partners. This is usually not the case for protein multilayers in conventional laminate structures; therefore, our approach opens the opportunity to reveal minor or even hidden changes in the protein upon stimulus.

Scheme 1. Reaction Scheme for the Chemical Functionalization of Germanium with Dextran Brushes

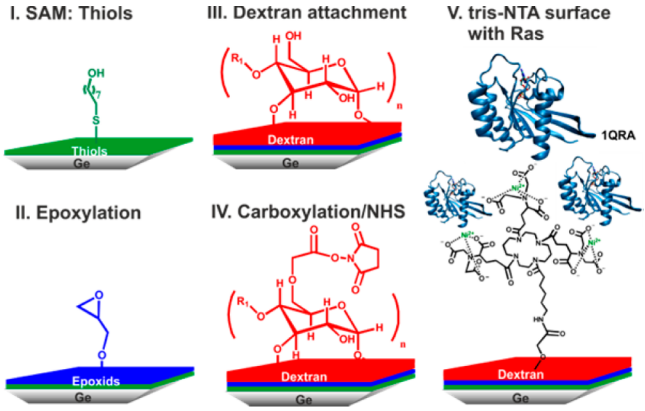

Dextran Coating of ATR Crystals. The preparation of germanium with self-assembled thiol monolayers was published previously.[32,33,35,36] Please note that our previous work was crucial for the establishment of dextran brushes on germanium because very basic conditions are required, and as we showed, thiol monolayers on germanium are stable under those conditions.[32] In contrast the previous silane modification would not allow working at highly basic conditions. We used monolayers of 8-mercaptooctanol, which were converted into epoxides using 1-chloro-2,3-epoxypropane. The obtained IR spectrum after washing the surface with water/ethanol is shown in (Figure S1, Supporting Information). The bands at 1264 and 1255 cm^{-1} can be assigned to the C−O stretching mode and the bands at 1080 cm^{-1}/1008 cm^{-1} to asymmetric/symmetric C−O−C stretching mode. The ring vibrations of the epoxide appear at 962 and 928 cm^{-1} (Supporting Information Figure S1). The desired dextran was flushed over the surface and reacted overnight.[14] The obtained spectra for covalently bound dextran brushes with molecular weights of 70 and 500 kDa are shown in Figure 1. The bands facing upward at 1158 and 1020 cm^{-1} correspond to the dextran brush and the bands facing downward at 960 and 929 cm^{-1} to the reacted epoxide ring vibration, which got substituted during the reaction. We observed the highest binding capacity (absorbance at 1020 cm^{-1}) for the 70 kDa dextran with 13.6 ± 2.7 mOD.

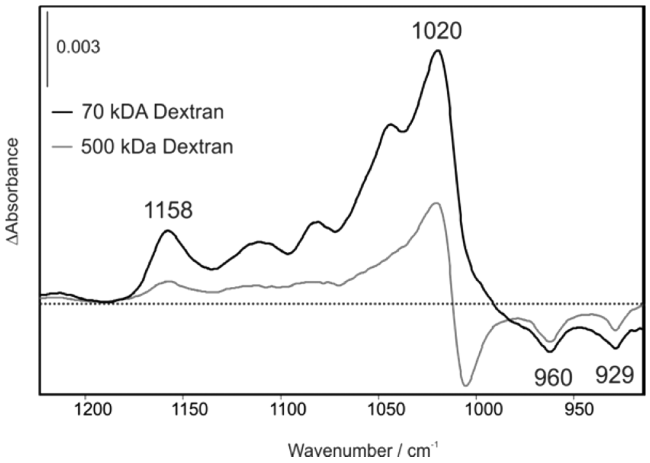

Figure 1. Spectra of the dextran attachment after a washing step. Only covalently bound dextran brushes remained stable on the ATR germanium crystal. The 70 kDa dextran showed the highest amount. The negative band at 1008 cm^{-1} corresponds to the epoxide (see Supporting Information Figure S1), but it is masked by the higher positive absorbance in case of the 70 kDa dextran.

The 500 kDa dextran showed a lower binding yield with 8.6 ± 2.8. Therefore, the 70 kDa was the most promising candidate for protein immobilization. This finding is consistence with a study of Monchaux and Vermette.[22] After the successful coating with the dextran, a functionlization is necessary for protein binding. Therefore, the hydroxy groups were carboxylated with bromoacetic acid. After a washing step with Millipore water, typical carboxylate vibrations are obtained (Supporting Information Figure S2). The band at 1580 cm^{-1} corresponds to the asymmetric stretching mode, and at 1400 cm^{-1} the symmetric stretching mode was observed (Supporting Information Figure S2). To activate the carboxylic acid residues NHS/EDC activation was performed.[37] The obtained spectrum after washing with MES buffer (pH 5) for 5 min is in accordance with our previously published results (Supporting Information Figure S3).[31] Subsequently, a NaP_i buffer (NaP_i, pH 5.4) was employed and a new reference spectrum was recorded. Immediately, a 50 mM ANTA solution (NaP_i, pH 5.4) was flushed over the surface. The bands at 1672 cm^{-1} (CO stretching mode) and 1587 cm^{-1} (NH bending, CN stretching) are characteristic for the formed peptide bond between the carboxylated dextran and ANTA (Supporting Information Figure S4A). The reaction was complete after about 1000 min as shown by the monoexponential fit in Supporting Information Figure S4B. We also tested a shorter reaction time (240 min), resulting in a similar amount of immobilized Ras (Supporting Information Figure S5). Since an acidic pH was used the hydrolysis of the NHS ester is decelerated. Finally, the surface was washed and incubated with 1 M ethanolamine (pH 8.5) to inactivate residual NHS esters. Subsequently, the Ni-

DOI: 10.1021/acs.analchem.5b01823
Anal. Chem. 2015, 87, 7467−7475

NTA groups were loaded with Ni^{2+} (30 mM $NiCl_2$, 10 min) and the surface was prepared for protein attachment.

Surface Characterization with AFM. For further characterization of the surface we employed AFM. The dextran-coated germanium crystals were measured in protein binding buffer 1 (pH 7.4). First, we compared the thickness of the 70 and 500 kDa dextran brushes. For the 500 kDa dextran brush we observed a thickness of 41 ± 6 nm (Supporting Information Figure S6). A thicker layer was detected for the 70 kDa dextran brush with 111 ± 29 nm (Supporting Information Figure S7). These findings are consistent with our ATR-FT-IR data, which showed the highest binding yield for 70 kDa dextran and a much lower for the 500 kDa dextran. The AFM measurements confirm the successful and stable chemical modification of germanium with dextran brushes. The measurements were done on surfaces with long carboxylation time of 16 h. The negative charge could explain the high thickness of the dextran brushes. That is why we tested the 70 kDa dextran with a shorter carboxylation time of 4 h (Figure 2A–D). This resulted in layer thickness of 53.5 ± 6.5 nm and is

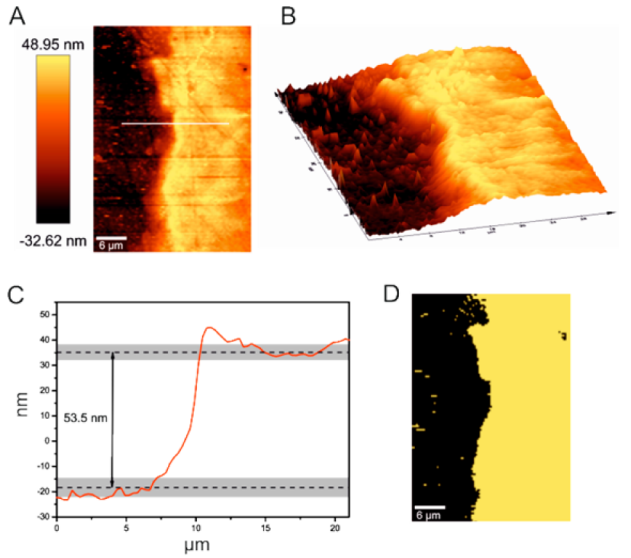

Figure 2. Characterization of a germanium crystal coated with a 70 kDa dextran brush (4 h carboxylated). (A) Topography of the substrate measured by AFM. The white line indicates the cross section shown in panel C. (B) 3D topographic image of the dextran-coated surface. (C) Cross section through the unmodified and dextran-coated germanium surface resulting in a thickness of 53.5 nm. (D) Image mask separating the dextran-coated germanium surface from the uncoated surface.

a clear hint concerning the charge effect (Figure 2A–D). To further investigate the effect of a negatively charged surface we measured the same surface at pH 3. Here, a decrease in the layer thickness of 22% was observed. With pH 11 the layer thickness was increased by 6%. The protonation at pH 3 reduces negative charges, and their repulsions inducing a shrinking of the dextran. The opposite effect was observed for pH 11, because the deprotonation increases the negative charge and induces a growing of the polymer.[38,39] This was also confirmed by ATR-FT-IR spectroscopic measurements, which showed negative dextran bands at high pH and positive bands a low pH (Supporting Information Figure S8). In ATR-FT-IR spectroscopy molecules that are closer to the surface as obtained by a shrinking process of the brush show a stronger absorbance. This effect is based on the exponential decay of the evanescent wave. The AFM measurements approved the successful dextran coating of germanium and enabled a detailed analysis of the layer thickness.

Protein Immobilization on Dextran Brushes. The dextran-coated ATR crystal was further characterized regarding protein immobilization. With the mono-NTA functionalized 500 kDa dextran brush we observed an amide 2 absorbance of 48.1 mOD for N-Ras1-180 with His-tag. The same experiment on the 70 kDa dextran yielded in an absorbance of 75.7 mOD for His-tagged N-Ras. Every 30 min the total concentration of N-Ras was raised by 1 μM to finally 5 μM after 150 min (black squares, Figure 3A). All further experiments were performed with the 70 kDa dextran, because besides the dextran layer thickness also the protein loading was increased. In the next step N-Ras1-180 without a His-tag was flushed over an unused

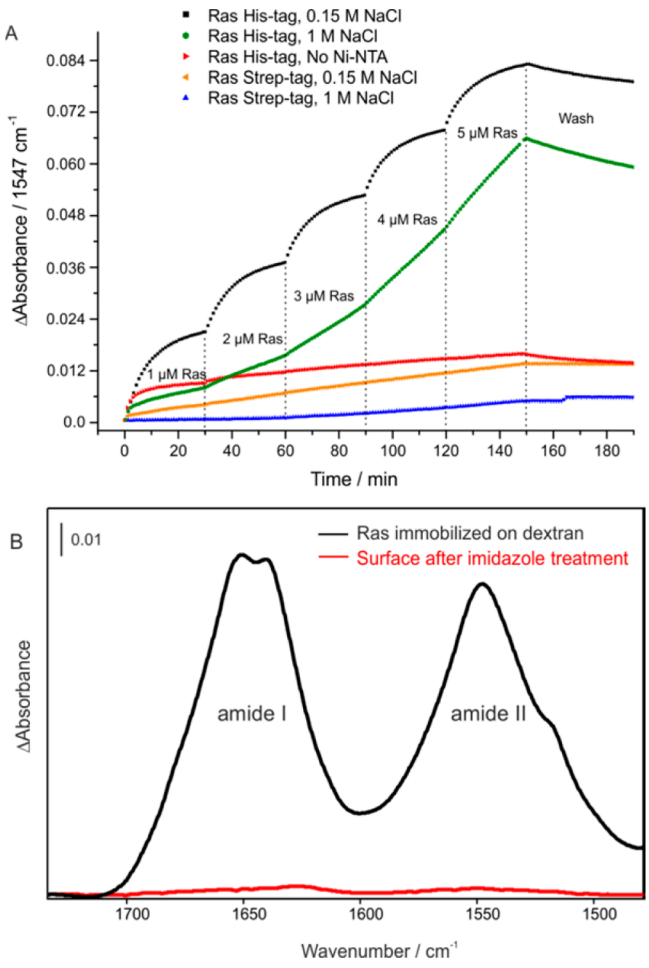

Figure 3. (A) Immobilization of Ras on dextran-coated ATR germanium crystals. N-Ras1-180 with Strep-tag was flushed over the surface under high salt (1 M NaCl, blue triangles, 4.7 mOD) and physiological salt (0.15 M NaCl, orange triangles, 14.2 mOD). Without Ni-NTA groups a similar amide 2 absorption was detected with 14.4 mOD (red triangles). N-Ras1-180 with His-tag under high salt yields in a higher amount of immobilized protein (60.0 mOD, green circles) and under physiological conditions the highest affinity toward the dextran surface with 75.7 mOD was observed (black squares). (B) Ras 3D layer on dextran-coated ATR germanium crystals. In black the characteristic amide 1 and amide 2 bands are shown. After imidazole treatment (500 mM imidazole, 150 mM NaCl) and a washing step almost all proteins were eluted.

DOI: 10.1021/acs.analchem.5b01823
Anal. Chem. 2015, 87, 7467–7475

dextran surface (orange triangles, Figure 3A). We observed an amide 2 absorbance of 14.2 mOD after 30 min rinsing with buffer 1. To verify the molecular reason for the protein binding the same experiment was performed under high salt condition (1 M NaCl), and the absorption decreased to 4.7 mOD. This indicates that about 10 mOD are probably bound through electrostatic interaction and the remaining 4.7 mOD (6.2%) are otherwise unspecifically bound proteins (blue triangles, Figure 3A). To further investigate the electrostatic effect we tested N-Ras1-180 with a C-terminal His-tag in the presence of 1 M sodium chloride. Besides a slight decrease in the stability, the amount of attached N-Ras (60.0 mOD) was much higher because of the specific immobilization via His-tag (green circles, Figure 3A). Under physiological conditions the amount of immobilized N-Ras was increased to 75.7 mOD (black squares, Figure 3A). A common method to quantify the amount of unspecific binding is to wash the surface with imidazole (500 mM), which removes all specifically bound proteins by disturbing the His-tag Ni-NTA interaction. In our experiment almost all protein was removed and a specificity of 97% was determined (Figure 3B).[27,31] Besides to the stepwise immobilization by increasing the amount of Ras and thereby enabling more binding, it is also possible to add a higher concentrated Ras solution (10 μM), which resulted in an absorbance of 69.6 mOD, which decayed to 58.5 mOD after 40 min (Supporting Information Figure S9). In an additional control N-Ras1-180 with His-tag was flushed over the dextran-coated surface directly after the carboxylation. Hence, no Ni-NTA groups are available, the immobilization of N-Ras is based on electrostatic interactions, and the amount of 14.4 mOD confirms this finding (red triangles, Figure 3). Ras immobilized due to electrostatic interactions can in part (about 25%) be removed by washing with 1 M NaCl. Please note that the difference in absorbance of N-Ras under physiological conditions and high salt conditions (15.7 mOD) is consistent to the amount of Ras bound by electrostatic interaction. This also shows the reuseability of the surface and enables the rebinding of His-tagged proteins. With the combination of dextran brushes and ATR germanium crystals the difference spectroscopy of proteins will now be more sensitive toward small changes within the studied protein. In our previous work we showed that Ras forms dense monolayers with an absorption of about 20 mOD.[31] This corresponds to about 1.3 μg of protein at the measured surface of roughly 3 cm^2. By establishing dextran brushes on germanium we increased the loading up to 145 mOD, when 400 μg of protein is offered (Supporting Information Figure S10). Please note that our setup is not finally optimized concerning the sample volume, which could probably reduce the required amount of sample. Neglecting the distance dependence of the signal, about 9 μg of protein is immobilized. Assuming a layer thickness of 100 nm a local concentration of 15 mM protein was estimated. Significant increase of the signal-to-noise ratio compared to a monolayer allows revealing also minor or hidden changes in the protein upon stimulus. As demonstrated by the AFM measurements a shorter carboxylation time reduces the dextran thickness. Furthermore, the amount of carboxylated dextran should be sufficient for immobilization, because also a shorter ANTA reaction time results in high Ras binding yields (Supporting Information Figure S5A). We analyzed the immobilization of N-Ras on such a surface (bromoacetic acid for 4 h). As shown in Supporting Information Figure S5A, the binding kinetics remained almost unchanged and also the stability and the amount are not negatively influenced. The ratio of amide 2 absorbance and amount of N-Ras gives also a hint that these conditions approximate a saturated value (Supporting Information Figure S5B). Our preferred protocol is in consistence with the work of Monchaux and Vermette.[22] Therefore, the upcoming experiments were performed with this improved protocol, which reduces the surface preparation time by 30%.

Tris-Ni-NTA for Protein Immobilization. A good biosensor is characterized by specificity, reusability, protein nativity, and also by stable immobilization of the protein. As shown in Figure 3 the N-Ras immobilization is sufficiently stable, but difference spectra are mixed with spectra from protein detachment. Thus, for the difference spectroscopy we aimed to further improve the stability by making use of multivalent binding through multiple NTA groups. Therefore, we synthesized tris-ANTA according to the literature.[28] A general synthesis scheme is shown in the Supporting Information (Scheme S1). Three of four binding sites of 1,4,8,11-tetraazacyclotetradecane (cyclam) were substituted with NTA branches, and the forth branch was substituted with an 6-aminohexanoic acid anchor. For the coupling of tris-ANTA the dextran was activated with EDC/NHS as already mentioned. After equilibration with sodium phosphate buffer (pH 5.4), a 4 mM solution of tris-ANTA was flushed over the surface and a new reference spectrum was recorded. In the CH region two main bands grow over time. We assign the band at 2961 cm^{-1} to the asymmetric stretching mode of the CH_2 groups in the cyclam and the second band at 2924 cm^{-1} to the asymmetric stretching mode of the aliphatic CH_2 groups (Figure 4A). During the reaction a new peptide bond is formed. Hence, we assign the band at 1663 cm^{-1} to the C═O stretching mode and the band at 1585 cm^{-1} to the NH bending/CN stretching mode (Figure 4B). We also observed a band in the carboxylic region (1410 cm^{-1}), which correspond to the symmetric stretching mode of carboxylates.[27] The reaction is complete after about 800 min as indicated by the monoexponential function (Figure 4C). The proceeding steps are the same as with mono-NTA. To analyze the Ni coordination of the three NTA branches a 50 mM K_2SO_4 solution at pH 4.8 was used.[27] After recording a reference spectrum a 50 mM $NiSO_4$ (in 50 mM K_2SO_4) was rinsed over the surface. The induced changes are caused by the coordination of Ni^{2+} by the three carboxylic group of each branch. The positive bands at 1588 cm^{-1} corresponds to asymmetric stretching mode of the carboxylate groups, and the symmetric vibration is found at 1410 cm^{-1} (green, Figure 5A). Thus, the Ni^{2+} binding induces changes in the carboxylic residues. This is assured by the negative bands at 1388 and 1356 cm^{-1}, which can be assigned to a combination of carboxylic, C−N, and C−H vibrations (green, Figure 5A).[27] To prove that these changes are caused by the Ni^{2+} ion, a new reference was taken and the surface was immersed with 50 mM ethylenediaminetetraacetic acid (EDTA) to remove the Ni ions. After washing with 50 mM K_2SO_4 pH 4.8 the red spectrum in Figure 5A was obtained, which is mirror-symmetric to the Ni coordination spectrum (green) and thus clearly shows that we monitored the complex formation between tris-NTA and Ni^{2+}. The nickel-loaded surface was then immersed with N-Ras1-180 His-tag with the conditions mentioned above. As shown in Supporting Information Figure S11 (normalized binding kinetics), the stability of Ras was slightly increased by use of tris-NTA (black) in comparison to mono-NTA (blue). In addition, the binding capacity of N-Ras increased, too. We

DOI: 10.1021/acs.analchem.5b01823
Anal. Chem. 2015, 87, 7467−7475

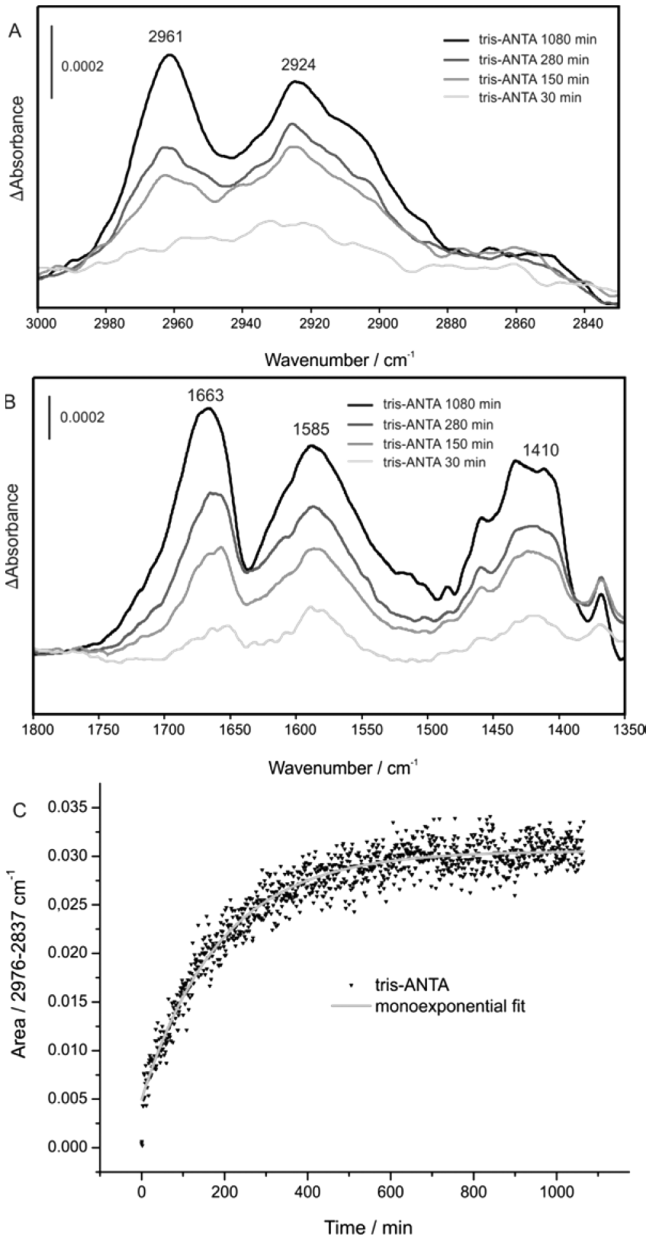

Figure 4. (A) ATR-FT-IR spectra of the NHS-activated dextran brush with tris-ANTA. We assign the band at 2961 cm^{-1} to the cyclic CH_2 groups in the cyclam and the second band at 2924 cm^{-1} to the aliphatic CH_2 groups. (B) The formed peptide bond is characterized by the amide 1 at 1663 cm^{-1} and amide 2 at 1585 cm^{-1}. Further the carboxylic acids show characteristic vibrations at in the region at 1410 cm^{-1}. (C) The reaction was revealed in real time and was complete after about 800 min (monoexponential fit).

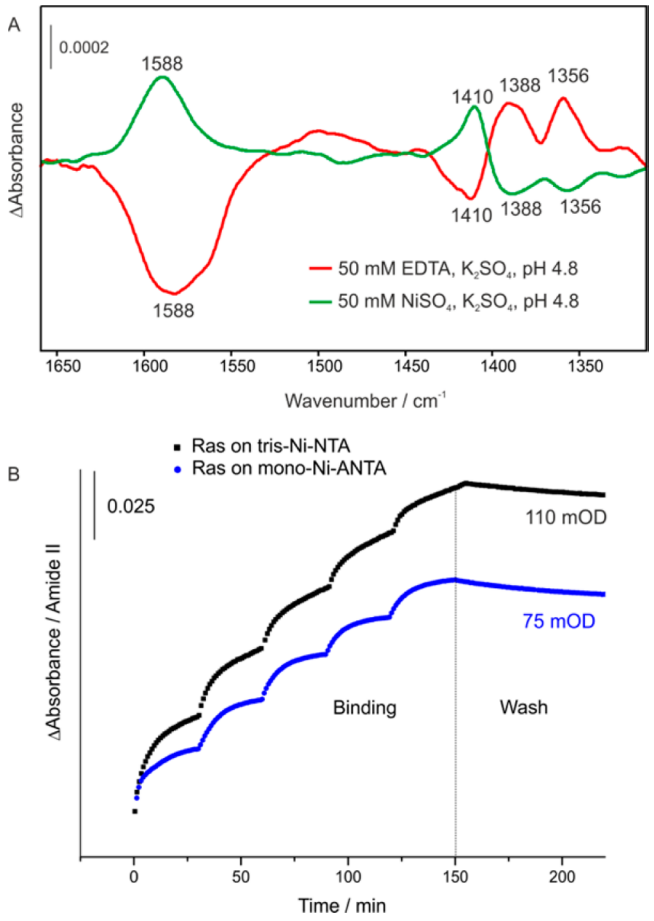

Figure 5. (A) Green spectrum shows the changes in the carboxylic acid residues of tris-NTA upon Ni^{2+} coordination. The changes can be reversed by removing Ni^{2+} with EDTA. (B) Binding kinetics of N-Ras1-180 His-tag on a 70 kDa dextran surface functionalized with mono-NTA (blue) and tris-NTA (black). The amount of immobilized N-Ras was increased when tris-NTA was employed.

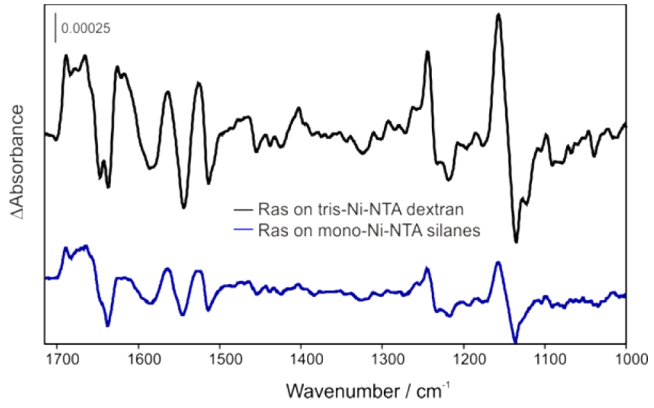

Figure 6. Stimulus-induced difference spectra of immobilized Ras on tris-Ni-NTA dextran brushes were obtained by a BeF_x assay. In comparison to our recent technique on Ni-NTA silanes a significant increase in the signal-to-noise ratio was achieved (factor of 3, ref 31).

observed an absorbance of 110 mOD (Figure 5B). This is a further advantage and reduces the required amount of protein sample. The unnormalized binding kinetics are shown in Figure 5B. The crucial step was to prove protein activity. Therefore, we added beryllium fluoride to mimic the ON-state of the Ras protein. BeF_3^- binds in the position of the γ-phosphate of Ras·GDP, and thus the GTP bound state is imitated. Positive bands correspond to the ON-state and negative bands to the OFF-state of the small GTPase (Figure 6). In comparison to Ras immobilized on a silane-based SAM with mono-Ni-NTA,[31] the difference signal upon stimulus of Ras immobilized to tris-Ni-NTA dextran was increased by factor 3 (Figure 6). Thus, the time to obtain the same S/N is reduced by 1 order of magnitude. Furthermore, this allows even for a quantitative evaluation of the movement of one single amino acid (Thr35, marker band) as revealed in the BeF_3^- titration assay (Supporting Information Figure S12).[40]

DOI: 10.1021/acs.analchem.5b01823
Anal. Chem. 2015, 87, 7467−7475

Fluorescence Microscopy. Our ATR cuvette is equipped with a quartz window that enables fluorescence measurements at the same time. To further analyze the surface we attached GFP by a hexahistidine tag. We added 2 μM GFP in NaP_i (pH 6.7) to the system and increased the total concentration every 15 min by 2 μM to finally 8 μM GFP. This resulted in an absorbance of 36.0 mOD. After a washing step the protein remained stable at 27.0 mOD (Supporting Information Figure S13A). This is over 3 times more than for a monolayer as we demonstrated with immobilized mCherry.[32] The amount of loosely bound protein that is flushed away is a bit higher, compared to N-Ras due to the shorter His-tag. When 4 μM GFP is added we obtained an absorbance of 32.2 mOD, and after rinsing with buffer 22 mOD remained stable (Supporting Information Figure S13B). Immobilized GFP was excited at 488 nm and an emission at 520 nm was detected (Figure 7). As

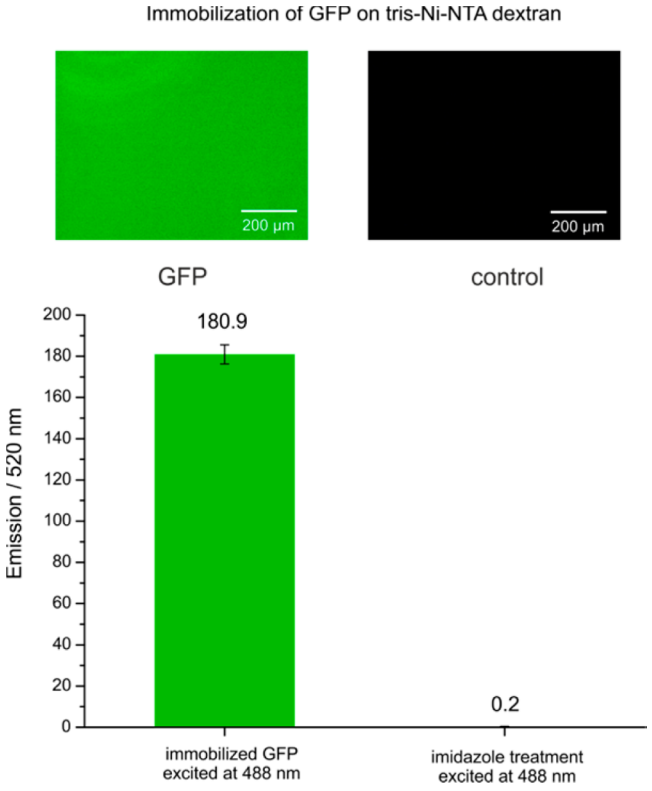

Figure 7. Immobilization of GFP on dextran brushes functionalized with tris-Ni-NTA branches. The germanium surface was exposed for 50 ms with a blue light source (488 nm), and a strong fluorescence was observed (520 nm). As a control experiment, the surface was washed with imidazole and almost no fluorescence was detected.

a control the surface was washed with imidazole (500 mM, 10 min), and no fluorescence was observed (Figure 7). Using fluorescence microscopy it is not possible to differentiate between inactive and detached protein. ATR-FT-IR spectroscopic measurements clearly revealed that the loss of fluorescence is due to the detachment of the protein.

Furthermore, GFP is distributed homogeneously on the dextran brushes within the resolution of the microscope. GFP showed activity for about 2 weeks. The fluorescence was decreased to 24% of the original fluorescence after 2 weeks. In the next step, we immobilized GFP simultaneously with the red fluorescent protein mCherry (both 2 μM). To determine the distance between GFP and mCherry we performed Förster resonance energy transfer (FRET) measurements. If both proteins are in close proximity we should observe FRET, since the Förster radius is about 5 nm.[41] The ratio between immobilized GFP and mCherry was determined by subtracting normalized reference spectra of the amide I (1700−1600 cm^{-1}) of GFP and mCherry from the amide I band during the simultaneous immobilization. In the beginning of the binding a ratio of 1:1 was observed, but after about 100 min the amount of GFP increased to 65% and mCherry decreased to 35% (Supporting Information Table S1). Since this ratio remained unchanged after washing the surface with protein binding buffer 2 (Supporting Information Table S1), GFP seems to have a better accessibility of the His-tag. We also tested the nativity of mCherry and excited at 585 nm resulting in a strong red fluorescence, which could be observed for almost 2 weeks (Supporting Information Figure S13). In contrast, excitation at 488 nm did not lead to any red emission from FRET, indicating a distance of the proteins larger than the Förster radius of 5 nm. The estimation of 2 mM protein in the dextran corresponds to a mean distance of about 9 nm if a homogeneous distribution of the proteins in the whole layer is assumed (for a detailed calculation see Supporting Information). An accumulation of a large part of the proteins at a certain region of the layer would lead to smaller distances, and FRET would be expected.[42] The homogeneous distribution excludes undesired protein−protein interactions of the immobilized proteins. In contrast, the same experiment on a Ni-NTA-thiol monolayer[32] results in a signal with 8.3% ± 1.9% of the total fluorescence in the red channel. With the quantum yield of mCherry of 22% taken into account this corresponds to a FRET of 38%.[41,43] This result is in accordance with a dense monolayer of randomly distributed fluorophores on a 2D surface using a calculation as described by Wolber and Hudson and Albertazzi et al.[41,44]

Comparison with Recent Techniques. The immobilization of proteins is required by SPR,[11−13] quartz crystal microbalance (QCM),[45−47] and surface acoustic waves (SAW).[48−50] These are very useful methods for the determination of affinities and binding kinetics, but no structural information is gained. For an understanding at the atomic level spectral resolution is indispensable. Another technique is the surface-enhanced infrared absorption spectroscopy (SEIRA) that provides spectral resolution and usually uses gold surfaces for immobilization.[51] An advantage of SEIRA is the possibility of performing cyclic voltammetry.[27] Nevertheless, the S/N ratio of the obtained difference spectra is worse compared to those of proteins immobilized on germanium.[32] Previous works showed protein binding on chemically modified germanium, but high-quality difference spectra were not reported.[52,53] For instance, a biosensor for the detection of coagulation factor VIII was developed.[54] Furthermore, the covalent attachment of a β-lactamase receptor via cysteine maleimido linkage on silane-modified germanium was investigated.[55] Specific attachment of lipidated N-Ras on germanium revealed the formation of a dimer on a POPC model membrane.[9] In addition, for the first time the extraction of a Rab protein by guanosine nucleotide dissociation inhibitor (GDI) was monitored.[10] So far protein immobilization on germanium was mainly achieved by silane chemistry. The proteins were bound covalently with NHS esters,[52,53,56] maleimido cysteine coupling,[55] or coordinatively with Ni-NTA.[31] The coupling conditions of dextran brushes to germanium needed a surface modification that is stable under basic conditions. Therefore, we employed thiol chemistry to

DOI: 10.1021/acs.analchem.5b01823
Anal. Chem. 2015, 87, 7467−7475

overcome this problem.[32] The high stability of thiols for biomolecule binding was also recently demonstrated by covalent binding of GFP.[33] Our approach enables the formation of a protein 3D layer and the investigation of proteins at atomic level under physiological conditions.

CONCLUSION

Here, we report on the chemical functionalization of germanium with dextran brushes. These dextran brushes allow for the first time stimulus-induced difference spectroscopy of a protein 3D layer in real time. Each reaction step was controlled within the spectrometer. All surfaces were characterized with AFM, and we showed that accumulation of negative charge within the dextran influences its thickness. The favorable dextran was the 70 kDa, because it forms the thickest layer and captures the highest amount of protein. With mono-NTA functionalized dextran brush this amount corresponds to several protein monolayers. The stability and loading was further improved by employing tris-NTA for protein immobilization. The surface has a specificity of 97% and can be easily reused by detaching proteins by imidazole treatment. Upon stimulus with the small molecule beryllium fluoride difference spectra with outstanding S/N ratios were obtained. Furthermore, we were able to immobilize His-tagged fluorescent proteins GFP and mCherry with the same setup. Both showed activity over weeks and demonstrated a homogeneous distribution on the dextran without any undesired protein−protein interactions. The immobilization via dextran brushes on germanium opens the opportunity to study the interaction of proteins with drugs, ligands, or other small molecules with a remarkable S/N ratio. Thus, our technique facilitates unraveling details in protein−drug interaction and binding kinetics.

ASSOCIATED CONTENT

Supporting Information

Figure S1, epoxylation of the thiol monolayer; Figure S2, carboxylation of the dextran; Figure S3, NHS/EDC activation of the surface; Figure S4, reaction with ANTA; Figure S5, analysis of different immobilization conditions with N-Ras; Figure S6, AFM measurements of the 500 kDa dextran; Figure S7, AFM measurements of the 70 kDa dextran; Figure S8, analysis of the dextran brushes under acidic and basic pH; Figure S9, immobilization of N-Ras at high concentrations; Scheme S1, synthesis of tris-ANTA; Figure S10, FT-IR spectrum of immobilized N-Ras (145 mOD); Figure S11, comparison of normalized mono-NTA and tris-NTA; Figure S12, BeF_x titration of the amino acid Thr35 of Ras; Figure S13, immobilization of GFP; Table S1, ratio of GFP and mCherry during the immobilization; Figure S13, fluorescence microscopy of immobilized mCherry. The Supporting Information is available free of charge on the ACS Publications website at DOI: 10.1021/acs.analchem.5b01823.

AUTHOR INFORMATION

Corresponding Author

*E-mail: carsten.koetting@rub.de.

Notes

The authors declare no competing financial interest.

ACKNOWLEDGMENTS

We thank Alexander Kutz for the GFP and Philipp Pinkerneil for the N-Ras protein. This work was performed in the framework of SFB 642 (German Research Foundation DFG, Sonderforschungsbereich 642, Projekt A1).

REFERENCES

(1) Kötting, C.; Gerwert, K. *ChemPhysChem* **2005**, *6* (5), 881−888.
(2) Kötting, C.; Gerwert, K. *Biol. Chem.* **2015**, *396* (2), 131−144.
(3) Kandori, H.; Furutani, Y.; Murata, T. *Biochim. Biophys. Acta* **2015**, *1847* (1), 134−141.
(4) Barth, A. *Prog. Biophys. Mol. Biol.* **2000**, *74* (3−5), 141−173.
(5) Gavriljuk, K.; Schartner, J.; Itzen, A.; Goody, R. S.; Gerwert, K.; Kötting, C. *J. Am. Chem. Soc.* **2014**, *136* (26), 9338−9345.
(6) Gavriljuk, K.; Gazdag, E.-M.; Itzen, A.; Kötting, C.; Goody, R. S.; Gerwert, K. *Proc. Natl. Acad. Sci. U. S. A.* **2012**, *109* (52), 21348−21353.
(7) Glassford, S. E.; Byrne, B.; Kazarian, S. G. *Biochim. Biophys. Acta, Proteins Proteomics* **2013**, *1834* (12), 2849−2858.
(8) Güldenhaupt, J.; Adigüzel, Y.; Kuhlmann, J.; Waldmann, H.; Kötting, C.; Gerwert, K. *FEBS J.* **2008**, *275* (23), 5910−5918.
(9) Güldenhaupt, J.; Rudack, T.; Bachler, P.; Mann, D.; Triola, G.; Waldmann, H.; Kötting, C.; Gerwert, K. *Biophys. J.* **2012**, *103* (7), 1585−1593.
(10) Gavriljuk, K.; Itzen, A.; Goody, R. S.; Gerwert, K.; Kotting, C. *Proc. Natl. Acad. Sci. U. S. A.* **2013**, *110* (33), 13380−13385.
(11) Liedberg, B.; Nylander, C.; Lunström, I. *Sens. Actuators* **1983**, *4*, 299−304.
(12) Vachali, P. P.; Li, B.; Bartschi, A.; Bernstein, P. S. *Arch. Biochem. Biophys.* **2014**, *572*, 66−72.
(13) Fischer, T.; Beyermann, M.; Koch, K.-W. *Biochem. Biophys. Res. Commun.* **2001**, *285* (2), 463−469.
(14) Löfas, S.; Johnsson, B. *J. Chem. Soc., Chem. Commun.* **1990**, *21*, 1526.
(15) Johnsson, B.; Löfås, S.; Lindquist, G. *Anal. Biochem.* **1991**, *198* (2), 268−277.
(16) Fortugno, C.; Varchi, G.; Guerrini, A.; Carrupt, P.-A.; Bertucci, C. *J. Pharm. Biomed. Anal.* **2014**, *95*, 151−157.
(17) Frazie, R. A.; Matthijs, G.; Davies, M. C.; Roberts, C. J.; Schacht, E.; Tendler, S. J. *Biomaterials* **2000**, *21* (9), 957−966.
(18) Mannelli, I.; Minunni, M.; Tombelli, S.; Wang, R.; Michela Spiriti, M.; Mascini, M. *Bioelectrochemistry* **2005**, *66* (1−2), 129−138.
(19) Bosker, W. T. E. *Brushes and Proteins*. Ph.D. Thesis, Wageningen University, 2011.
(20) Lee, S.; Pérez-Luna, V. H. *Anal. Chem.* **2005**, *77* (22), 7204−7211.
(21) Dubiel, E. A.; Vermette, P. *Colloids Surf., B* **2012**, *95*, 266−273.
(22) Monchaux, E.; Vermette, P. *Langmuir* **2007**, *23* (6), 3290−3297.
(23) Monchaux, E.; Vermette, P. *Biomacromolecules* **2007**, *8* (11), 3668−3673.
(24) Ishida, K. P.; Griffiths, P. R. *J. Colloid Interface Sci.* **1993**, *160* (1), 190−200.
(25) Porath, J.; Carlsson, J.; Olsson, I.; Belfrage, G. *Nature* **1975**, *258* (5536), 598−599.
(26) Hochuli, E.; Döbeli, H.; Schacher, A. *J. Chromatogr. A* **1987**, *411*, 177−184.
(27) Ataka, K.; Giess, F.; Knoll, W.; Naumann, R.; Haber-Pohlmeier, S.; Richter, B.; Heberle, J. *J. Am. Chem. Soc.* **2004**, *126* (49), 16199−16206.
(28) Lata, S.; Reichel, A.; Brock, R.; Tampé, R.; Piehler, J. *J. Am. Chem. Soc.* **2005**, *127* (29), 10205−10215.
(29) Lata, S.; Piehler, J. *Nat. Protoc.* **2006**, *1* (4), 2104−2109.
(30) Lata, S.; Piehler, J. *Anal. Chem.* **2005**, *77* (4), 1096−1105.
(31) Schartner, J.; Güldenhaupt, J.; Mei, B.; Rögner, M.; Muhler, M.; Gerwert, K.; Kötting, C. *J. Am. Chem. Soc.* **2013**, *135* (10), 4079−4087.
(32) Schartner, J.; Gavriljuk, K.; Nabers, A.; Weide, P.; Muhler, M.; Gerwert, K.; Kötting, C. *ChemBioChem* **2014**, *15* (17), 2529−2534.

DOI: 10.1021/acs.analchem.5b01823
Anal. Chem. 2015, 87, 7467−7475

(33) Cai, Q.; Xu, B.; Ye, L.; Tang, T.; Huang, S.; Du, X.; Bian, X.; Zhang, J.; Di, Z.; Jin, Q.; Zhao, J. *Appl. Surf. Sci.* **2014**, *316*, 46−53.
(34) Danne, L.; Aktas, M.; Gleichenhagen, J.; Grund, N.; Wagner, D.; Schwalbe, H.; Hoffknecht, B.; Metzler-Nolte, N.; Narberhaus, F. *Mol. Microbiol.* **2015**, *95* (2), 313−331.
(35) Han, S. M.; Ashurst, W. R.; Carraro, C.; Maboudian, R. *J. Am. Chem. Soc.* **2001**, *123* (10), 2422−2425.
(36) Lommel, M.; Hönicke, P.; Kolbe, M.; Müller, M.; Reinhardt, F.; Möbus, P.; Mankel, E.; Beckhoff, B.; Kolbesen, B. O. *Solid State Phenom.* **2009**, *145*−*146*, 169−172.
(37) Wissink, M. J.; Beernink, R.; Pieper, J.; Poot, A.; Engbers, G. H.; Beugeling, T.; van Aken, W.; Feijen, J. *Biomaterials* **2001**, *22* (2), 151−163.
(38) Liu, Z. Q.; Wei, Z.; Zhu, X. L.; Huang, G. Y.; Xu, F.; Yang, J. H.; Osada, Y.; Zrínyi, M.; Li, J. H.; Chen, Y. M. *Colloids Surf., B* **2015**, *128C*, 140−148.
(39) Mocanu, G.; Nichifor, M. *Carbohydr. Polym.* **2014**, *99*, 235−241.
(40) Kötting, C.; Kallenbach, A.; Suveyzdis, Y.; Eichholz, C.; Gerwert, K. *ChemBioChem* **2007**, *8* (7), 781−787.
(41) Albertazzi, L.; Arosio, D.; Marchetti, L.; Ricci, F.; Beltram, F. *Photochem. Photobiol.* **2009**, *85* (1), 287−297.
(42) Day, R. N.; Davidson, M. W. *BioEssays* **2012**, *34* (5), 341−350.
(43) Shaner, N. C.; Campbell, R. E.; Steinbach, P. A.; Giepmans, B. N. G.; Palmer, A. E.; Tsien, R. Y. *Nat. Biotechnol.* **2004**, *22* (12), 1567−1572.
(44) Wolber, P. K.; Hudson, B. S. *Biophys. J.* **1979**, *28* (2), 197−210.
(45) Cai, Q.; Xu, B.; Ye, L.; Di, Z.; Zhang, J.; Jin, Q.; Zhao, J.; Xue, J.; Chen, X. *Talanta* **2014**, *120*, 462−469.
(46) Spera, R.; Festa, F.; Bragazzi, N. L.; Pechkova, E.; LaBaer, J.; Nicolini, C. *J. Proteome Res.* **2013**, *12* (12), 5535−5547.
(47) Wu, C.; Du, L.; Zou, L.; Huang, L.; Wang, P. *Analyst* **2013**, *138* (20), 5989−5994.
(48) Slamnoiu, S.; Vlad, C.; Stumbaum, M.; Moise, A.; Lindner, K.; Engel, N.; Vilanova, M.; Diaz, M.; Karreman, C.; Leist, M.; Ciossek, T.; Hengerer, B.; Vilaseca, M.; Przybylski, M. *J. Am. Soc. Mass Spectrom.* **2014**, *25* (8), 1472−1481.
(49) Cui, J.; Iturri, J.; Götz, U.; Jimenez, M.; del Campo, A. *Langmuir* **2013**, *29* (22), 6582−6587.
(50) Länge, K.; Rapp, B. E.; Rapp, M. *Anal. Bioanal. Chem.* **2008**, *391* (5), 1509−1519.
(51) Ataka, K.; Kottke, T.; Heberle, J. *Angew. Chem., Int. Ed.* **2010**, *49* (32), 5416−5424.
(52) Devouge, S.; Conti, J.; Goldsztein, A.; Gosselin, E.; Brans, A.; Voué, M.; De Coninck, J.; Homblé, F.; Goormaghtigh, E.; Marchand-Brynaert, J. *J. Colloid Interface Sci.* **2009**, *332* (2), 408−415.
(53) Voue, M.; Goormaghtigh, E.; Homble, F.; Marchand-Brynaert, J.; Conti, J.; Devouge, S.; De Coninck, J. *Langmuir* **2007**, *23* (2), 949−955.
(54) Goldzstein, A.; Aamouche, A.; Homblé, F.; Voué, M.; Conti, J.; De Coninck, J.; Devouge, S.; Marchand-Brynaert, J.; Goormaghtigh, E. *Biosens. Bioelectron.* **2009**, *24* (7), 1831−1836.
(55) Hammaecher, C.; Joris, B.; Goormaghtigh, E.; Marchand-Brynaert, J. *Eur. J. Org. Chem.* **2013**, *2013* (35), 7952−7959.
(56) Devouge, S.; Salvagnini, C.; Marchand-Brynaert, J. *Bioorg. Med. Chem. Lett.* **2005**, *15* (13), 3252−3256.

DOI: 10.1021/acs.analchem.5b01823
Anal. Chem. 2015, 87, 7467−7475

Supporting Information

Chemical Functionalization of Germanium with Dextran-Brushes for Immobilization of Proteins Revealed by ATR-FTIR Difference Spectroscopy

Jonas Schartner[1], Nina Hoeck[1], Jörn Güldenhaupt[1], Laven Mavarani[1], Andreas Nabers[1], Klaus Gerwert[1], Carsten Kötting[1,*]

[1]Department of Biophysics, Faculty of Biology and Biotechnology, Ruhr-University Bochum, Germany.

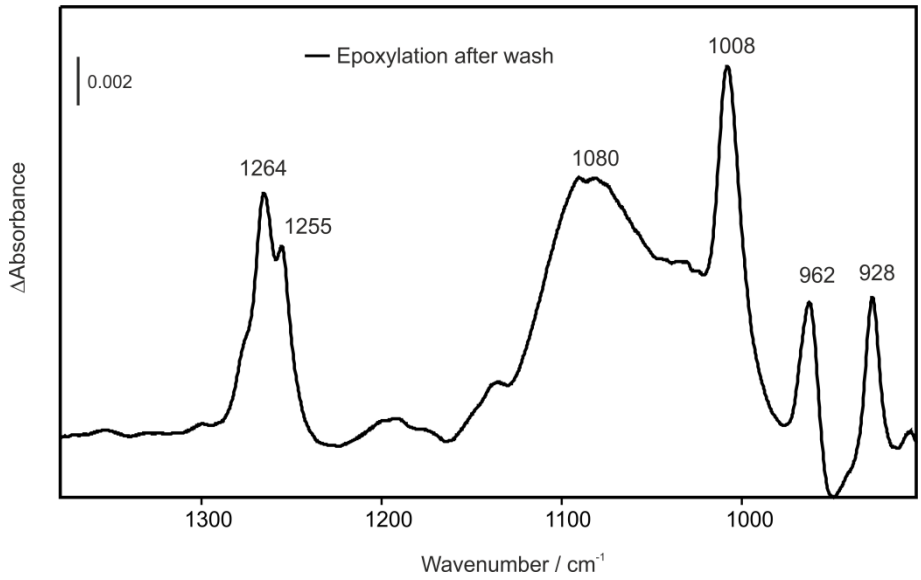

Figure S1: At first the germanium surface was epoxylated with epichlorohydrin. The surface was washed with water and ethanol. The obtained spectrum confirms the successful activation of germanium.

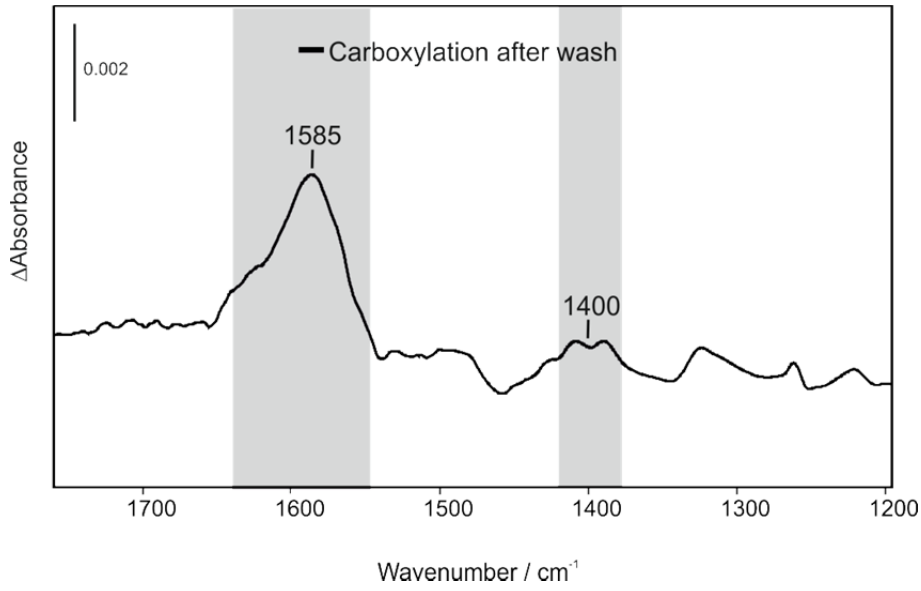

Figure S2: The immobilized dextran-brush was treated with bromoacetic acid and a carboxylated surface was obtained. After washing with water (pH 7) the characteristic bands for carboxylic acids remained.

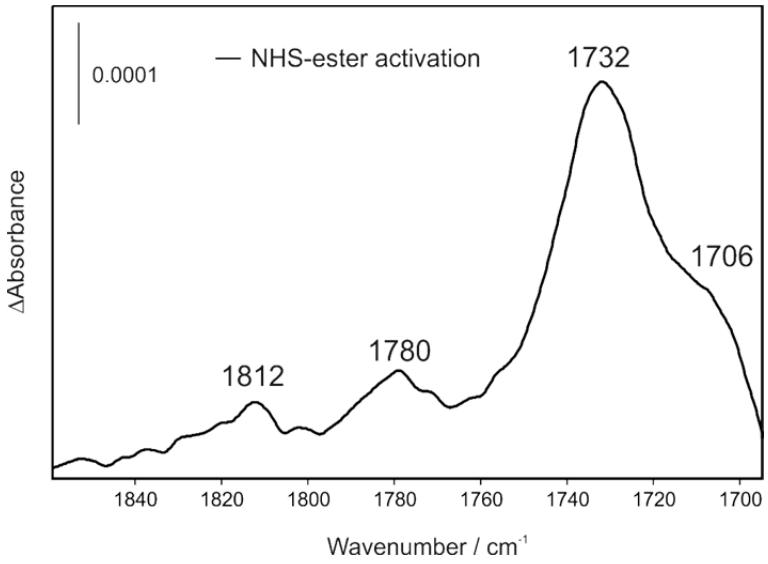

Figure S3: The carboxylated dextran-brush was incubated with EDC/NHS to form NHS-esters. The spectrum showed the typical bands for NHS-esters, which remained after rinsing the surface with water.

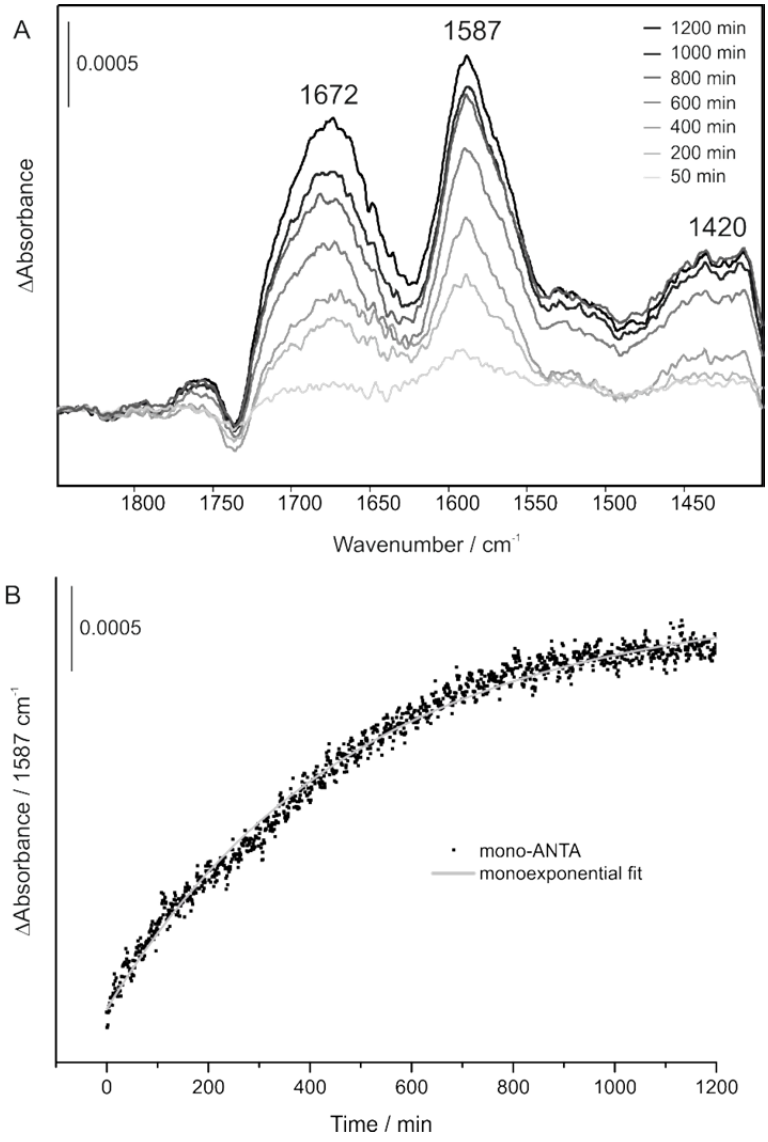

Figure S4: (A) Reaction of mono-ANTA with the NHS activated dextran. The formed peptide bond was characterized by the amide 1 and amide 2. (B) Kinetics of the reaction with mono-ANTA.

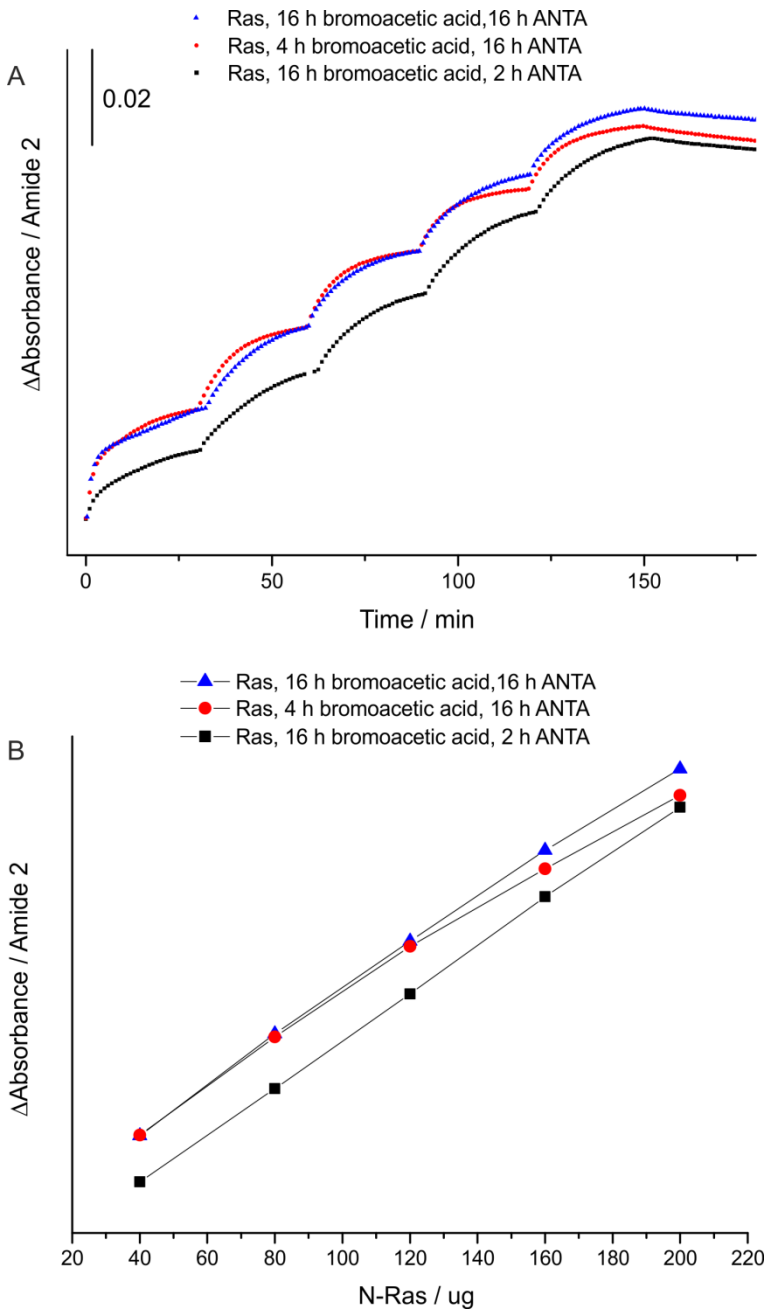

Figure S5: (A) Binding kinetics of N-Ras1-180 His-tag on a 70 kDa dextran surface with different carboxylation and ANTA reaction times. The binding kinetics were very similar and in all cases protein multilayers were obtained. (B) Plot of the amide 2 absorbance against the amount of offered Ras showed that a 4 h carboxylation time (red) and an ANTA coupling overnight were favorable.

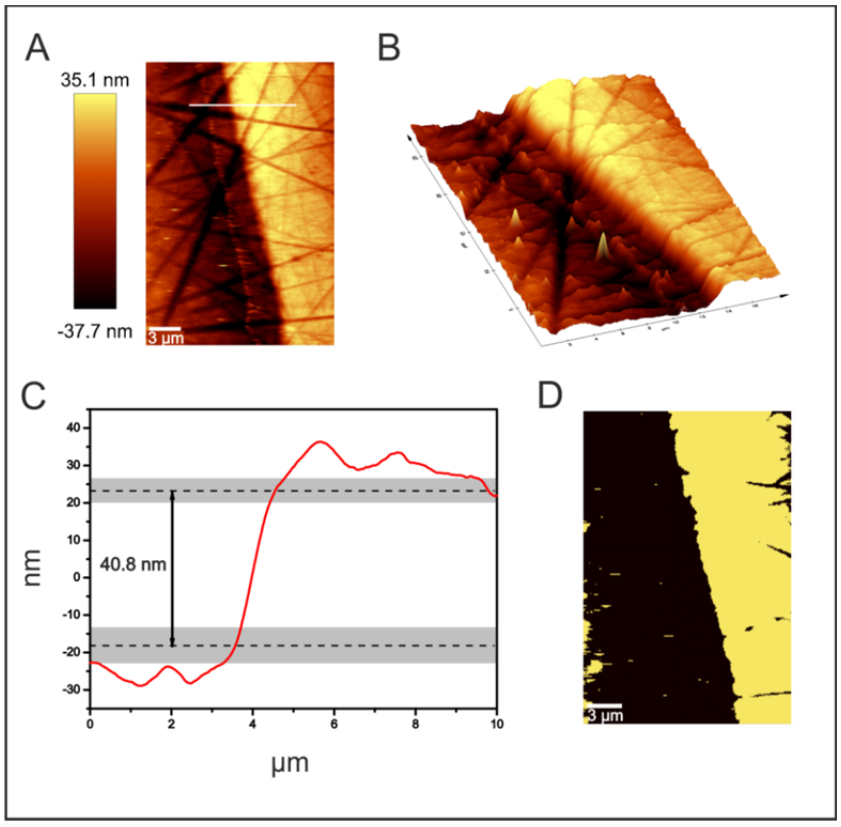

Figure S6: Characterization of a germanium crystal coated with a 500 kDa dextran (16 h carboxylated). (A) Topography of the substrate measured by AFM. The white line indicates the cross section shown in C. (B) 3D topographic image of the dextran coated surface. (C) Cross section through the unmodified and dextran coated germanium surface resulting in a thickness of 40.8 nm. (D) Image mask separating the dextran coated germanium surface from the uncoated surface.

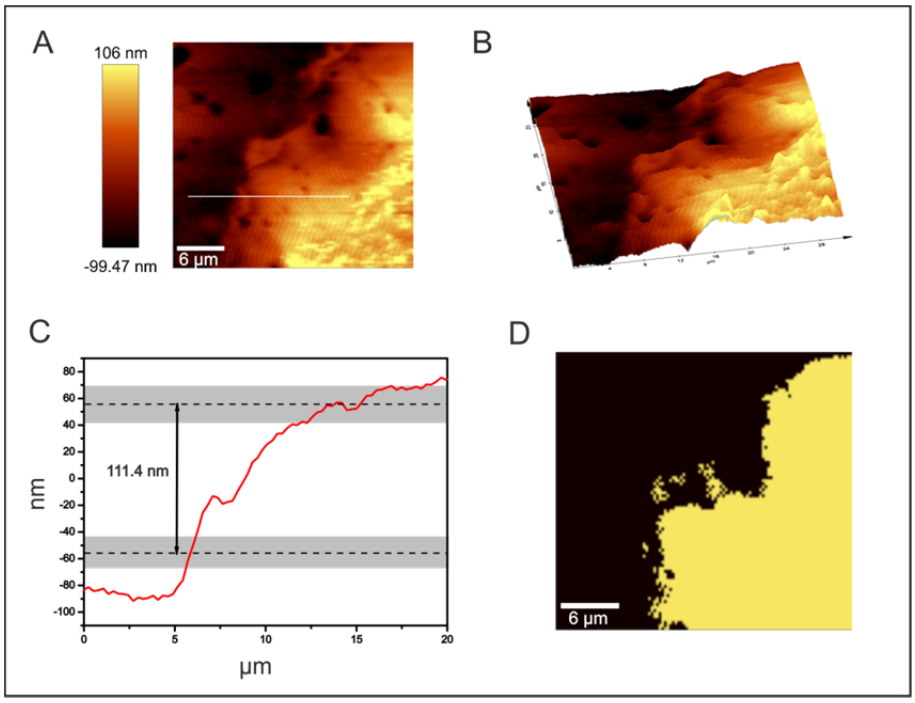

Figure S7: Characterization of a germanium crystal coated with a 70 kDa dextran (16 h carboxylated). (A) Topography of the substrate measured by AFM. The white line indicates the cross section shown in C. (B) 3D topographic image of the dextran coated surface. (C) Cross section through the unmodified and dextran coated germanium surface resulting in a thickness of 111.4 nm. (D) Image mask separating the dextran coated germanium surface from the uncoated surface.

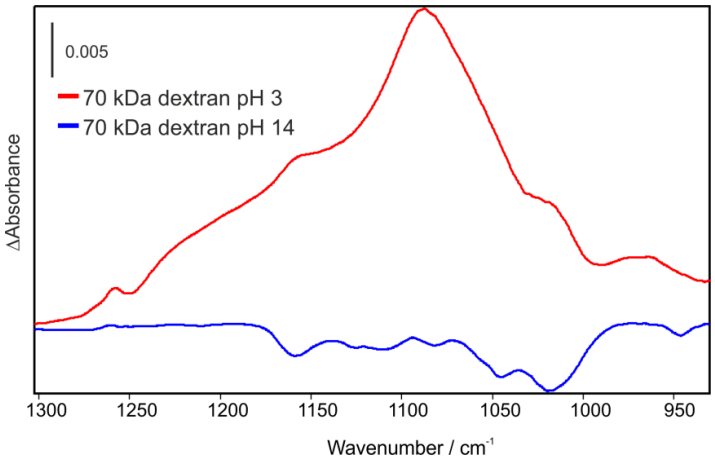

Figure S8: Analysis of the 70 kDa dextran under acidic pH 3 (red) and basic pH 14 (blue). The positive bands were induced by shrinking of the layer due to the protonation of the dextran. Negative bands (blue) were caused by a growing of the dextran-brush, which was induced by the charge repulsion caused by deprotonation of the hydroxyl-groups.

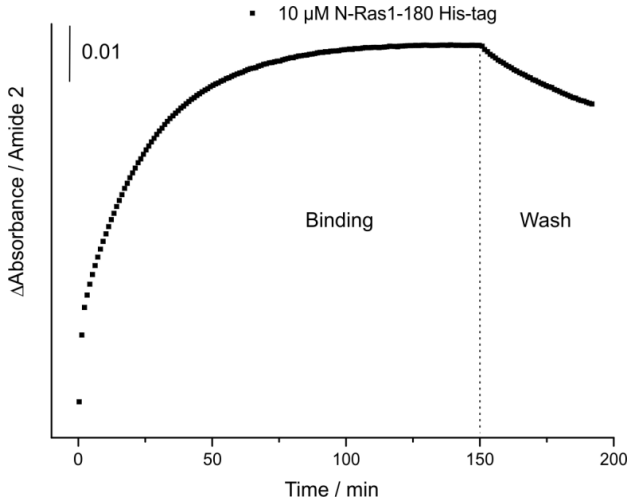

Figure S9: Binding kinetics of 10 µM N-Ras1-180 His-tag on a 70 kDa dextran surface.

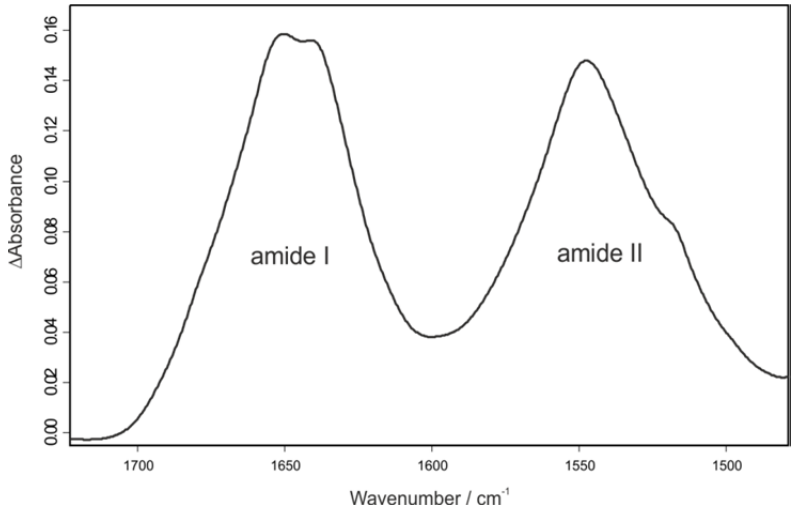

Figure S10: FTIR spectrum of immobilized Ras on a 70 kDa dextran-brush. An absorbance 145 mOD was observed after offering 400 µg of protein.

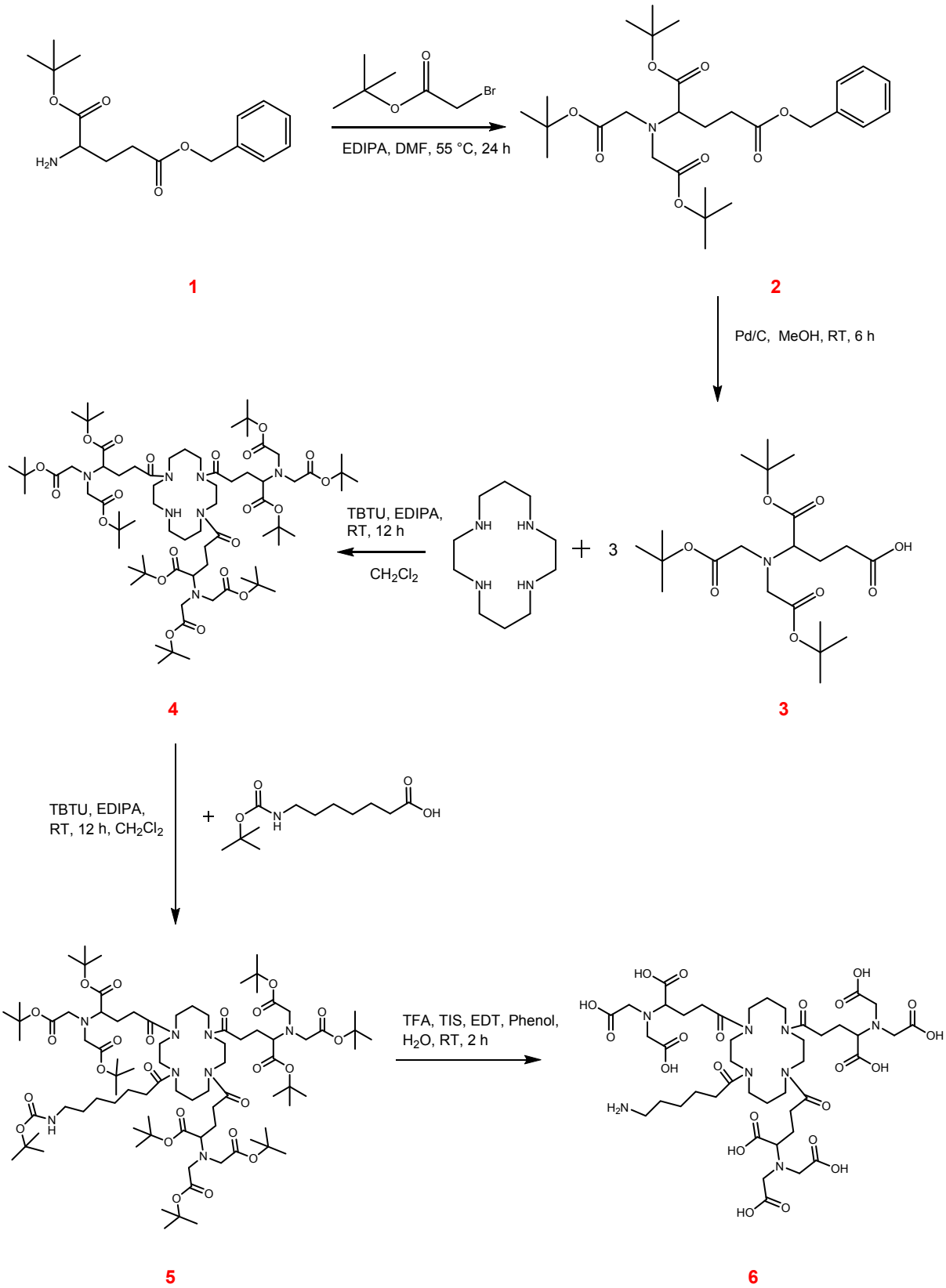

Scheme S1: Organic synthesis of tris-ANTA based on Lata et al..[1] Used chemicals were N,N-Diisopropylethylamine (EDIPA), Dimethylformamide (DMF), Palladium on carbon (Pd/C), Methanol (MeOH), O-(Benzotriazol-1-yl)-N,N,N′,N′-tetramethyluronium tetrafluoroborate (TBTU), Trifluoroacetic acid (TFA), Triisopropylsilane (TIS), 1,2-Ethanedithiol (EDT).

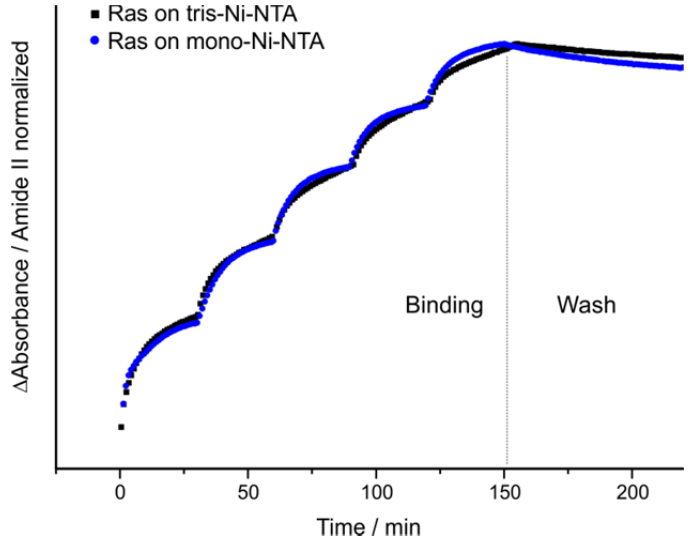

Figure S11: Comparison of the Ras immobilization on mono-Ni-NTA dextran (blue) with tris-Ni-NTA dextran (black). The protein stability was slightly increased.

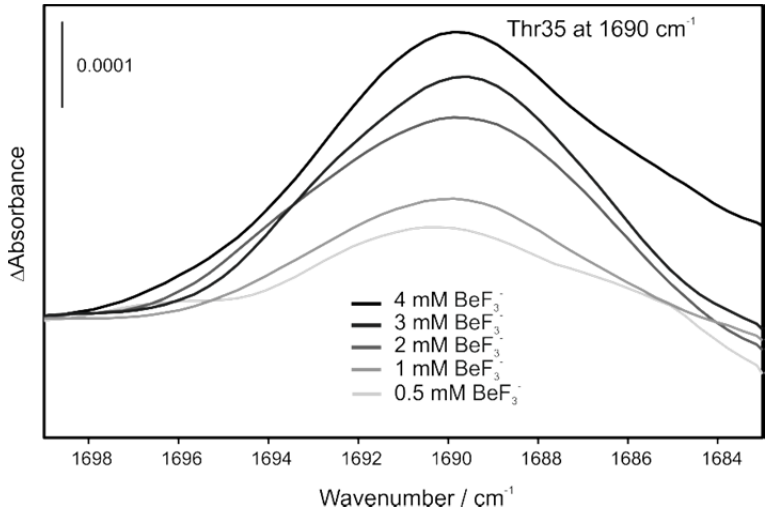

Figure S12: BeF_3^--titration of molecular changes of the amino acid Thr35 of Ras. The spectrum was additionally baseline corrected in the analyzed region to isolate the absorbance changes of Thr35.

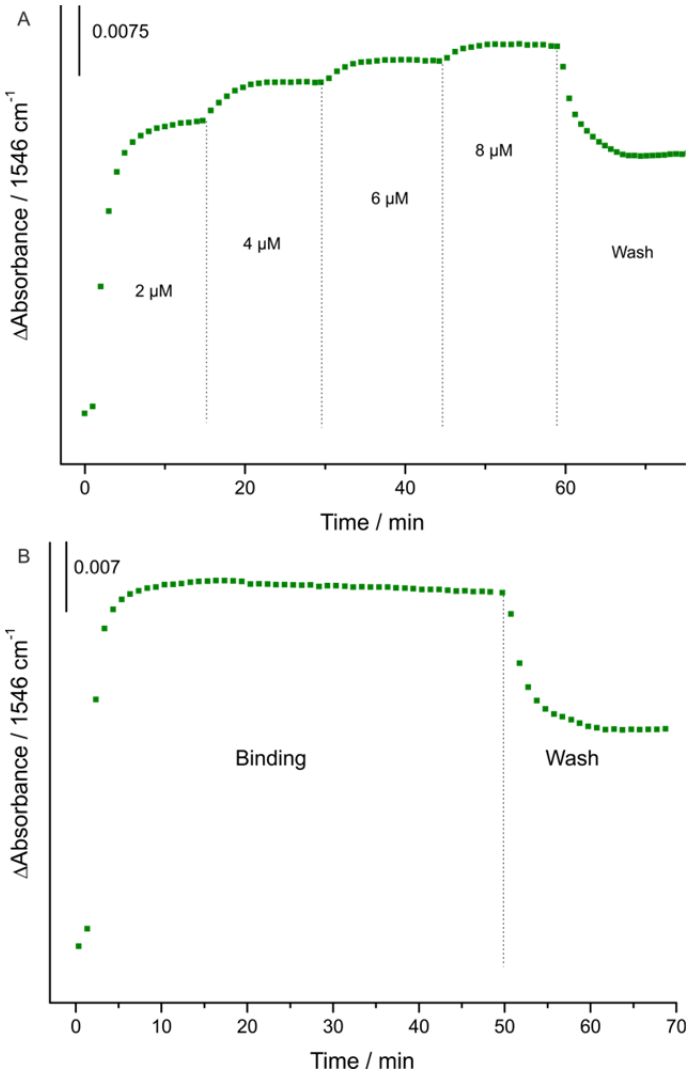

Figure S13: Binding kinetics of GFP with His-tag on a 70 kDa dextran surface functionalized with tris-ANTA. (A) The GFP concentration was successive increased (total concentration 8 µM). (B) A 4 µM GFP solution was employed and the binding monitored over time.

Table S1: Ratio of GFP and mCherry during the immobilization on a 70 kDa dextran surface functionalized with tris-ANTA.

Time	GFP / %	mCherry / %
Binding 5 min	47	53
Binding 30 min	51	49
Binding 60 min	56	44
Binding 90 min	60	40
Binding 105 min	65	35
After washing (2 h total)	65	35

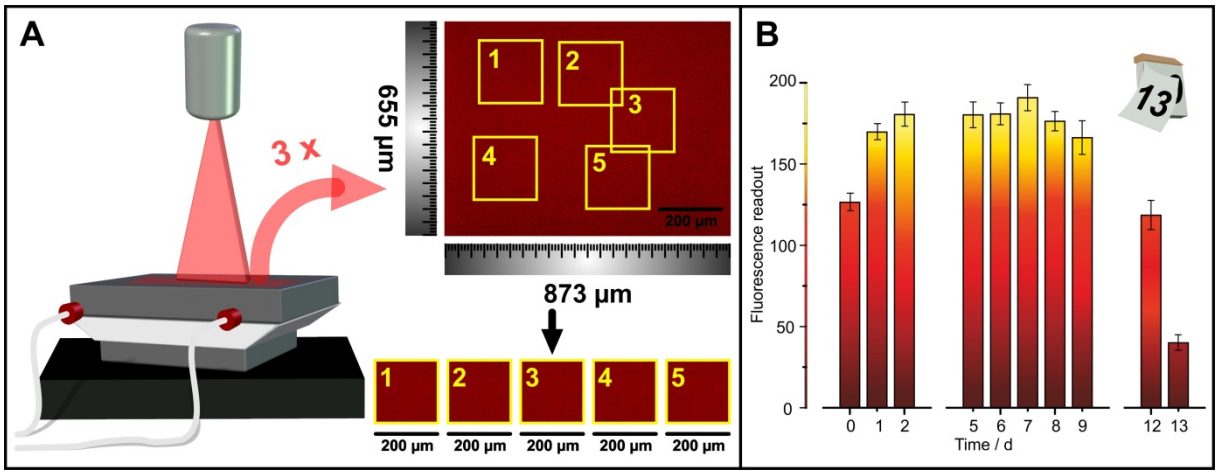

Figure S13: (A) Fluorescence microscopy of immobilized mCherry on a 70 kDa dextran surface functionalized with mono-ANTA. (B) Fluorescence intensity observed over days.

Calculation of the surface concentration for Ras:

The surface concentration of a Ras monolayer was deduced from the literature.[2] The measured surface area is 3 cm^2.

(1) $n(Ras\_monolayer) = 20\frac{pmol}{cm^2} \times 3cm^2 = 60\,pmol$

(2) $m(Ras\_monolayer) = 60\,pmol \times 20000\frac{g}{mol} = 1.3\mu g$

(3) $m(Ras\_dextran) = 435\,pmol \times 20000\frac{g}{mol} = 8.7\mu g$

Calculation of the surface concentration for mCherry and GFP:

The surface concentration of all mCherry present in the 3D-layer projected to the surface was calculated using formulas from the literature.[3] Equation 4 is the projection of the whole protein amount to the surface.

(4) $n(mCherry\_GFP\_dextran) = 22\frac{pmol}{cm^2} \times 3cm^2 = 66\,pmol$

(5) $c(mCherry\_GFP\_dextran) = \frac{66\,pmol}{0.0003m^2 \times 0.0000001m} l = 2.2\frac{mol}{m^3}$

The average distance is the cubic root of the volume per molecule:

(6) $d(mCherry\_GFP\_dextran) = \sqrt[3]{\frac{1}{2.2\frac{mol}{m^3} \times N_A}} = \sqrt[3]{\frac{1}{1.32 \times 10^{24}}} = 9nm$

References:

(1) Lata, S., Reichel, A., Brock, R., Tampé, R., and Piehler, J. (2005) High-Affinity Adaptors for Switchable Recognition of Histidine-Tagged Proteins. *Journal of the American Chemical Society 127*, 10205–10215.

(2) Schartner, J., Güldenhaupt, J., Mei, B., Rögner, M., Muhler, M., Gerwert, K., and Kötting, C. (2013) Universal method for protein immobilization on chemically functionalized germanium investigated by ATR-FTIR difference spectroscopy. *J. Am. Chem. Soc. 135*, 4079–4087.
(3) Schartner, J., Gavriljuk, K., Nabers, A., Weide, P., Muhler, M., Gerwert, K., and Kötting, C. (2014) Immobilization of Proteins in their Physiological Active State at Functionalized Thiol Monolayers on ATR-Germanium Crystals. *Chembiochem 15*, 2529–2534.